Innovative: International Multi-disciplinary Journal of Applied Technology
(ISSN 2995-486X) VOLUME 4 ISSUE 10, 2026

THERMAL ACTIVATION OF TEBINBULAK TITANOMAGNETITE ORE AS A LOW-COST MAGNETIC SORBENT PRECURSOR: TEMPERATURE–TIME DEPENDENCE OF SPECIFIC SURFACE AREA, CRYSTALLITE GROWTH AND PHASE STABILITY

Ergashev Muhsinjon Ergashevich
Department of Agronomy, Navoi State University of Mining and Technologies, Navoi, Uzbekistan

Shodiqulov Jurabek Mehriqulovich
Department of Agronomy, Navoi State University of Mining and Technologies, Navoi, Uzbekistan
shodiqulov_jurabek@mail.ru

Doniyorov Kamoliddin Alouddinovich
Department of Agronomy, Navoi State University of Mining and Technologies, Navoi, Uzbekistan

Abstract:

Natural titanomagnetite can serve as a precursor of magnetically recoverable iron-oxide sorbents, provided that its low initial surface area (≈4–7 $m^2 g^{-1}$) is developed without destroying the magnetite phase. Here the thermal activation of titanomagnetite ore from the Tebinbulak deposit (Karakalpakstan, Uzbekistan) was mapped over a full 6 × 5 factorial grid of temperature (500–1000 °C) and holding time (0.5–2.5 h), and the response of BET surface area, crystallite size, external surface and pore volume was described with empirical models. Surface area obeyed $S_{BET} = -83.1 + 15.8 \ln T + 3.60 \ln t$ ($R^2 = 0.976$), with first-order time saturation (τ = 0.31–0.45 h) and a limiting value S_∞ that grows from 17.2 to 27.8 $m^2 g^{-1}$ between 500 and 1000 °C. Crystallite size followed a power law $d \propto T^{1.31} t^{0.12}$ ($R^2 = 0.992$), i.e. coarsening is governed by temperature far more than by time. The surface gained per nanometre of crystallite growth ($\Delta S/\Delta d$) dropped eightfold, from 0.42 to 0.05 $m^2 g^{-1} nm^{-1}$, across the 500–1000 °C range, with the steepest fall above 700 °C, where the maghemite-to-hematite transformation of magnetite is known to accelerate. Combining these trends, 700 °C for 2.0 h is identified as the upper practical limit of activation: it provides 84 % of the thermally attainable surface (23.67 $m^2 g^{-1}$, external 18.80 $m^2 g^{-1}$, pore volume 0.120 $cm^3 g^{-1}$) at a crystallite size of 64.86 nm, with the product still predominantly in the

spinel phase. The models provide design equations for a sorbent intended for removing Mo, Se, U, As and V oxyanions from saline drainage water.

Keywords: titanomagnetite; thermal activation; BET surface area; grain growth; magnetite oxidation; empirical model; magnetic sorbent; Tebinbulak.

Introduction

Irrigated agriculture in the lower Amu Darya basin increasingly depends on the reuse of collector–drainage and shallow groundwater [1][2][3]. In the Kyzylkum region these waters combine high salinity (8.2–8.5 g L^{-1} dry residue) with molybdenum, selenium and uranium at 1.1–14 times the FAO/WHO guideline levels [4],[5]. Because these elements occur as oxyanions at circum-neutral pH [6][7], they pass through conventional lime or caustic precipitation and require a dedicated sorption step.

Among candidate sorbents, magnetite stands out because it unites three functions: inner-sphere complexation of oxyanions at ≡Fe–OH sites [8][9][10][11], reduction of U(VI), Se(IV/VI) and V(V) by lattice Fe^{2+} to sparingly soluble forms [12][13][14][15], and ferrimagnetism, which allows the loaded sorbent to be recovered in a low-field magnetic separator and reused [16][17]. The literature on magnetite sorbents, however, is dominated by synthetic nanoparticles tested in dilute solutions [18][19]; the preparation of a comparable material from a natural ore for use in brackish water has received little attention.

The Tebinbulak deposit in the Karauzyak district of Karakalpakstan holds 3.5–4.3 Gt of titanomagnetite ore (15–17 % Fe, upgradable to 63.5 % Fe by magnetic separation) [20] and has not previously been considered as a sorbent feedstock. The ore's vanadium content (V_2O_5 ≈ 0.15 %, 0.60–0.63 % in concentrate) is incidentally a reminder of the affinity of its surface for vanadate.

Converting the ore into a sorbent requires activation. Mechanical activation in high-energy mills creates surface area quickly and introduces lattice defects; thermal treatment removes water, dehydroxylates the surface and opens closed pores. The thermal route is attractive for its simplicity and for the stability of the surface it produces, but it carries two penalties that grow with temperature: grain coarsening (sintering) and the oxidation of magnetite in air, which proceeds through maghemite to hematite and removes both the Fe^{2+} and the strong magnetisation on which the sorbent concept depends. The problem is therefore one of locating, on a quantitative basis, the temperature–time region in which surface development outpaces these penalties.

In this study the full temperature–time response of four textural descriptors of thermally activated Tebinbulak ore was measured on a 30-point factorial grid and reduced to empirical equations. The objectives were (i) to obtain design relationships $S_{BET}(T, t)$ and $d(T, t)$, (ii) to define a criterion for the "cost" of surface in terms of crystallite growth, and (iii) to fix the upper limit of activation compatible with the retention of magnetite.

Materials and methods

Titanomagnetite ore from Tebinbulak, crushed to −20 mm and ball-milled to powder, was used throughout. Its composition and that of the magnetic concentrate are given in Table 1. Reference properties of the magnetite phase used in the interpretation: cubic spinel structure, density ≈5.0–5.2 g cm^{-3}, BET area of the raw ore ≈4–7 m^2 g^{-1}, point of zero charge 6.5 (6–6.8), amphoteric ≡Fe–OH surface groups.

Table 1. Composition of Tebinbulak ore and magnetic concentrate [20,21].

Parameter	Raw ore	Magnetic concentrate
Fe, wt %	15–17	63.5
TiO_2, wt %	2–3	4.50–4.64
V_2O_5, wt %	≈0.15	0.60–0.63
Main minerals	titanomagnetite, Fe_3O_4, $FeTiO_3$	—
Reserves, Gt	3.5–4.3	—

Samples were calcined in air in a laboratory muffle furnace on a full factorial grid: six temperatures (500, 600, 700, 800, 900, 1000 °C) × five isothermal holding times (0.5, 1.0, 1.5, 2.0, 2.5 h), 30 regimes in all. The grid brackets the temperature ranges reported for the maghemite and hematite transformations of magnetite. After the hold, samples cooled inside the furnace and were kept in a desiccator.

Each sample was characterised by (i) BET surface area from nitrogen adsorption; (ii) crystallite (particle) size, nm; (iii) external surface area, i.e. the fraction of the surface open to adsorbate, and (iv) pore volume, $cm^3\ g^{-1}$, both by the BJH treatment of the nitrogen isotherm. The magnetite/maghemite/hematite ratio was not quantified directly (no XRD was available for this series; the phase state is discussed on the basis of published oxidation kinetics and of the sintering behaviour, and is treated as a constraint rather than as a measured variable.

Three empirical descriptions were fitted to the 30-point data set by least squares. The temperature–time dependence of surface area and crystallite size was represented by

$$S_{BET} = a + b\ln T + c\ln t$$

$$\ln d = a' + b'\ln T + c'\ln t$$

the second being a power law $d \propto T^{b'}\ t^{c'}$ of the type used for grain growth. The isothermal time dependence of surface area at each temperature was fitted by first-order saturation,

$$S_{BET}(t) = S_\infty\left(1 - e^{-t/\tau}\right)$$

where S_∞ is the limiting area at that temperature and τ the characteristic time. The exchange rate between surface gain and grain growth was expressed, for consecutive 100 °C steps of the 2.0 h series, as

$$\varphi = \frac{\Delta S_{BET}}{\Delta d}$$

and the accessibility of the surface as the external fraction $f_{ext} = S_{ext}/S_{BET}$.

Results and Discussion

The complete surface-area grid is given in Table 2 and plotted in Fig. 1. Over the grid the area spans 11.76–28.20 $m^2\ g^{-1}$, a three- to fivefold increase over the raw ore. Two features of the response determine everything that follows. First, the dependence on temperature is concave: a plot against ln *T* is close to linear, and the regression $S_{BET} = -83.1 + 15.8\ \ln T + 3.60\ \ln t$ reproduces all 30 points with $R^2 = 0.976$ and a root-mean-square error of 0.67 $m^2\ g^{-1}$. The ratio of the two coefficients (15.8 versus 3.60) shows that a given relative change in temperature is worth about 4.4 times the same relative change in time.

Table 2. BET surface area, $m^2\ g^{-1}$, after thermal activation.

T, °C	0.5 h	1.0 h	1.5 h	2.0 h	2.5 h
500	11.76	14.70	16.66	16.92	17.26
600	15.68	18.62	20.58	20.88	21.12
700	18.62	21.56	23.52	23.67	24.04
800	19.95	22.80	24.70	25.38	26.22
900	21.85	24.70	26.60	27.26	27.26
1000	22.80	25.65	27.55	28.20	28.20

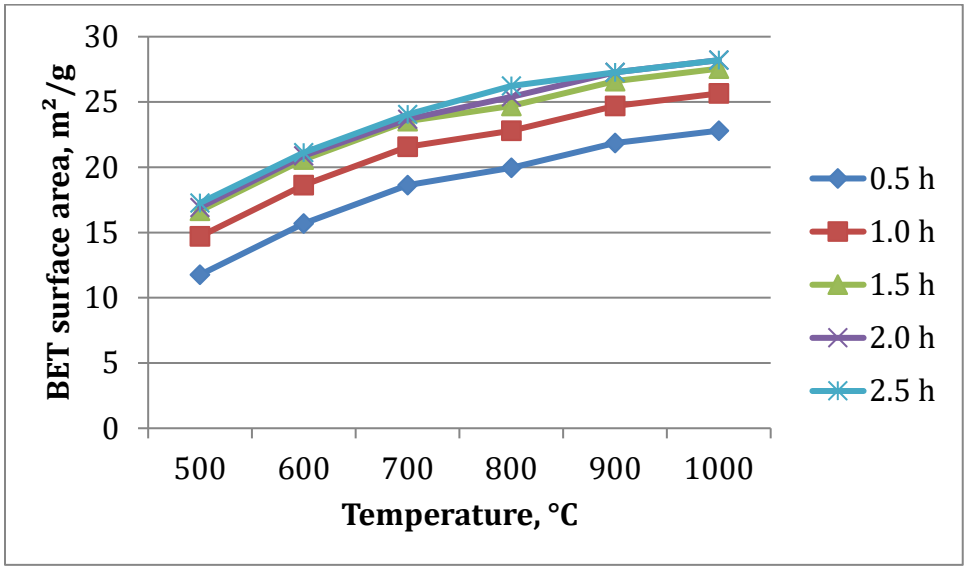


Fig. 1. BET surface area of thermally activated Tebinbulak titanomagnetite versus temperature for holding times of 0.5–2.5 h.

Second, the time dependence saturates early. First-order fits to the five isothermal points at each temperature (Table 3) give characteristic times τ of 0.45 h at 500 °C decreasing to 0.31 h at 900–1000 °C, so that 95 % of the limiting area is reached within 3τ ≈ 1.0–1.4 h at every temperature. The limiting area S_∞ itself rises from 17.2 to 27.8 m² g⁻¹ between 500 and 1000 °C, but with a steadily shrinking increment: the surface added by each successive 100 °C step of the 2.0 h series (Table 4, Fig. 2) falls from 3.96 m² g⁻¹ (500→600 °C) to 0.94 m² g⁻¹ (900→1000 °C). In other words, two thirds of the surface that temperature can add above 500 °C is already obtained by 700 °C, and the last three steps together yield less than the first one.

Table 3. Parameters of first-order saturation $S_{BET}(t) = S_\infty(1 - e^{-t/\tau})$ at each temperature.

T, °C	S_∞, m² g⁻¹	τ, h	3τ, h
500	17.16	0.45	1.35
600	20.89	0.38	1.14
700	23.69	0.34	1.02
800	25.36	0.35	1.05
900	26.90	0.31	0.93
1000	27.83	0.31	0.93

Table 4. Surface added per 100 °C step, 2.0 h series.

Interval, °C	500→600	600→700	700→800	800→900	900→1000
ΔS_{BET}, m² g⁻¹	3.96	2.79	1.71	1.88	0.94

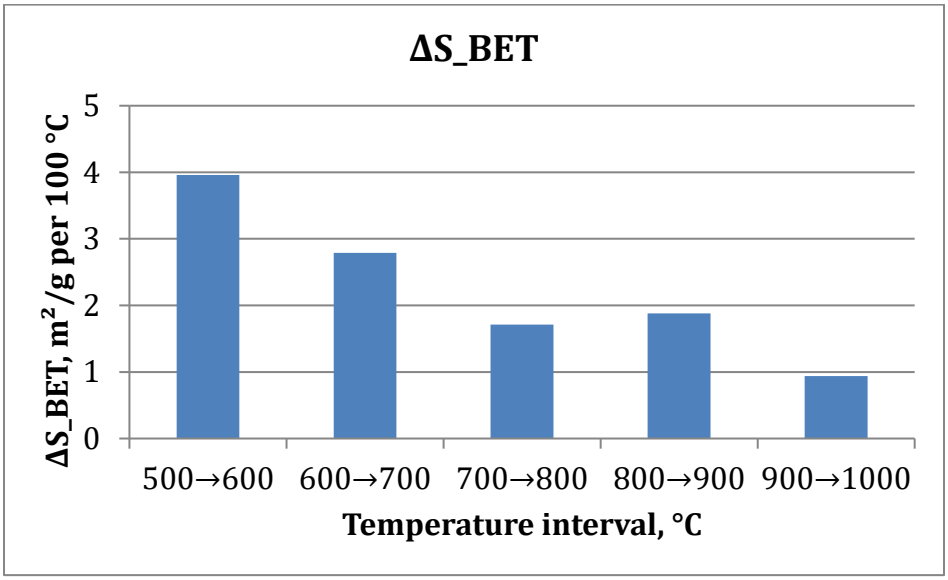


Fig. 2. Surface added per 100 °C step at a holding time of 2.0 h.

The physical reading of these two features is consistent with the dehydration–dehydroxylation mechanism of thermal activation: the processes that open porosity (loss of adsorbed and structural water, micro-cracking accompanying the volume change of oxidation) are fast at any temperature above 500 °C, which explains the short τ, whereas the amount of porosity that can be opened is finite and is approached asymptotically as temperature rises.

Crystallite size (Table 5, Fig. 3) behaves in the opposite way to surface area: it increases over the whole grid, from 37 nm (500 °C, 0.5 h) to 113 nm (1000 °C, 2.5 h), and its temperature dependence is convex rather than concave. The power-law regression $\ln d = -4.45 + 1.31 \ln T + 0.12 \ln t$ describes the data with $R^2 = 0.992$. The temperature exponent of 1.31 and the time exponent of 0.12 quantify what the raw numbers suggest: a 10 % rise in temperature enlarges the crystallites by about 13 %, whereas a 10 % extension of the hold adds only 1 %. The small time exponent is typical of grain growth controlled by boundary migration in oxide ceramics and indicates that, once a temperature is chosen, little is gained or lost in crystallite size by adjusting the hold.

Table 5. Crystallite/particle size, nm, after thermal activation.

T, °C	0.5 h	1.0 h	1.5 h	2.0 h	2.5 h
500	37.24	41.16	44.10	44.18	45.12
600	45.08	49.98	53.90	53.58	54.52
700	54.88	60.76	64.68	64.86	65.80
800	64.60	71.25	76.00	78.02	79.90
900	77.90	85.50	90.25	92.12	94.00
1000	93.10	102.60	108.30	110.92	112.80

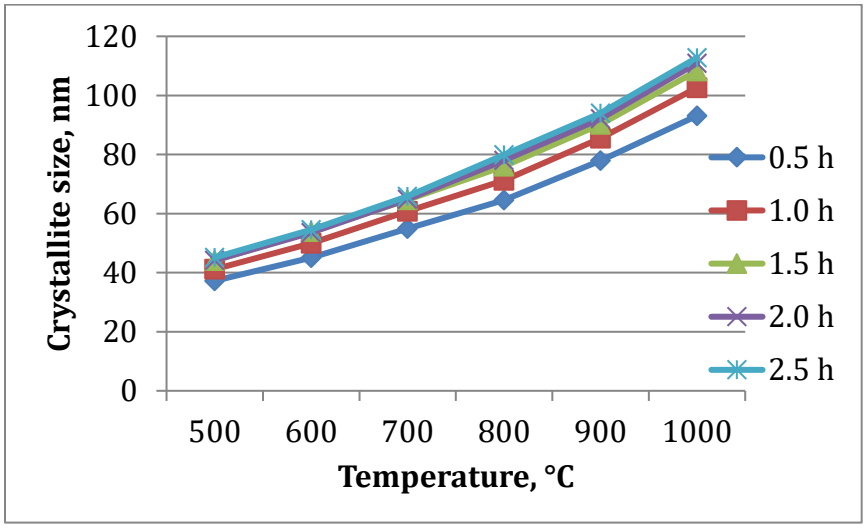


Fig. 3. Crystallite size versus activation temperature at holding times of 0.5–2.5 h.

That surface area and crystallite size rise together is only an apparent paradox. If the particles were dense spheres, a growth from 44 to 111 nm would halve the specific surface; the observed doubling instead shows that the area being measured is internal — pores and cracks opened inside grains that are at the same time merging with their neighbours. The two descriptors therefore report two different processes, porosity opening and grain coalescence, and the useful question is at what temperature the second begins to outweigh the first.

External surface and pore volume

The external surface (Table 6) and pore volume (Table 7, Fig. 4) track the BET area closely. The external surface rises from 8.82 to 22.76 $m^2\ g^{-1}$, and the external fraction f_{ext} stays within 75–80 % over the entire grid (79.4 % at 700 °C/2.0 h), so that four fifths of the surface created thermally is open to adsorbate. The remaining 20–25 % is internal porosity, a larger share than in mechanically activated ore (≈11 %), consistent with the porosity-opening origin of the thermal surface. Pore volume rises from 0.039 to 0.150 $cm^3\ g^{-1}$, with the same concave temperature dependence as the area: 0.120 $cm^3\ g^{-1}$ is reached at 700 °C/2.0 h, and the three further steps to 1000 °C add only 0.027 $cm^3\ g^{-1}$.

Table 6. External (active) surface area, $m^2\ g^{-1}$, after thermal activation.

T, °C	0.5 h	1.0 h	1.5 h	2.0 h	2.5 h
500	8.82	11.76	12.74	13.16	14.10
600	11.76	14.70	16.66	16.72	16.92
700	14.70	17.64	18.62	18.80	19.74
800	16.15	18.05	19.95	20.28	20.68
900	17.10	19.95	20.90	21.32	21.72
1000	18.05	20.90	21.85	22.36	22.76

Table 7. Pore volume, $cm^3\ g^{-1}$, after thermal activation.

T, °C	0.5 h	1.0 h	1.5 h	2.0 h	2.5 h
500	0.039	0.059	0.069	0.075	0.078
600	0.059	0.078	0.088	0.094	0.103
700	0.078	0.098	0.118	0.120	0.122
800	0.086	0.114	0.126	0.130	0.132
900	0.095	0.124	0.133	0.138	0.141
1000	0.105	0.133	0.143	0.147	0.150

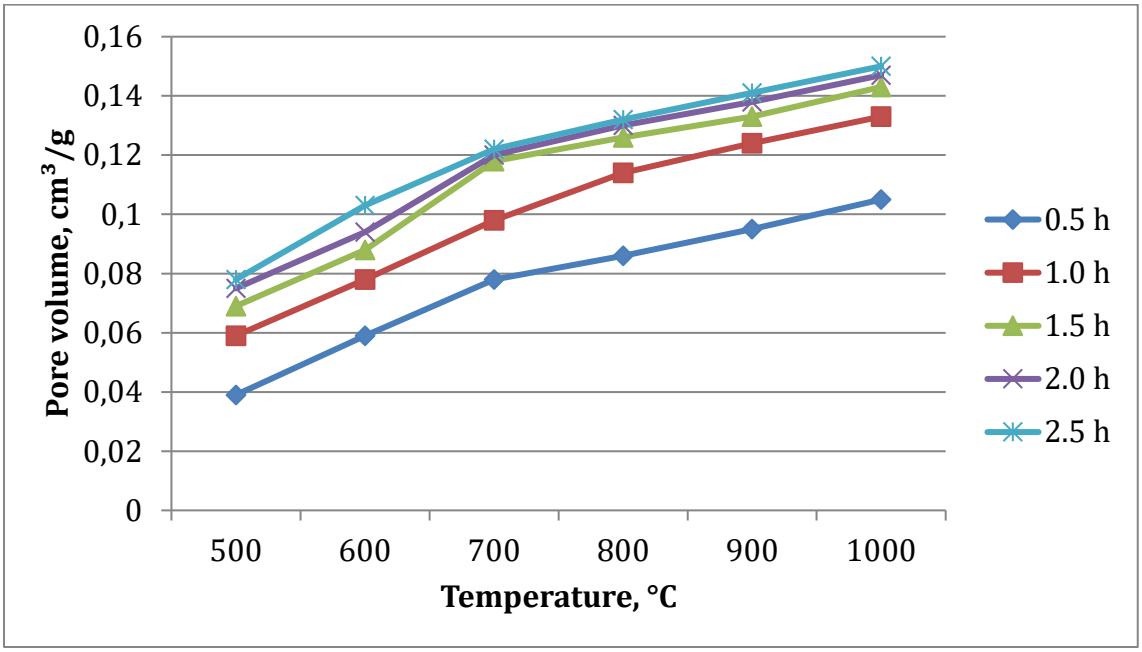


Fig. 4. Pore volume versus temperature at holding times of 0.5–2.5 h.

Because the two penalties of high temperature — coarsening and oxidation — both scale with crystallite growth, the most informative single criterion is the surface gained per unit of growth, $\varphi = \Delta S_{BET}/\Delta d$, evaluated step by step along the 2.0 h series (Table 8, Fig. 5). φ falls monotonically from 0.42 $m^2\ g^{-1}\ nm^{-1}$ for the 500→600 °C step to 0.05 $m^2\ g^{-1}\ nm^{-1}$ for 900→1000 °C — an eightfold decline — and the sharpest drop occurs between the 600→700 and 700→800 °C steps, where φ halves. The cumulative ratio S_{BET}/d tells the same story: it peaks at 0.39 $m^2\ g^{-1}\ nm^{-1}$ at 600 °C, is still 0.37 at 700 °C and then declines to 0.25 at 1000 °C.

Table 8. Surface gain, crystallite growth and their ratio φ per 100 °C step, 2.0 h series.

Interval, °C	ΔS_{BET}, $m^2\ g^{-1}$	Δd, nm	$\varphi = \Delta S/\Delta d$, $m^2\ g^{-1}\ nm^{-1}$	S_{BET}/d at upper T	S_{BET}/S_{max} at upper T, %
500→600	3.96	9.40	0.42	0.390	74.0
600→700	2.79	11.28	0.25	0.365	83.9
700→800	1.71	13.16	0.13	0.325	90.0
800→900	1.88	14.10	0.13	0.296	96.7
900→1000	0.94	18.80	0.05	0.254	100.0

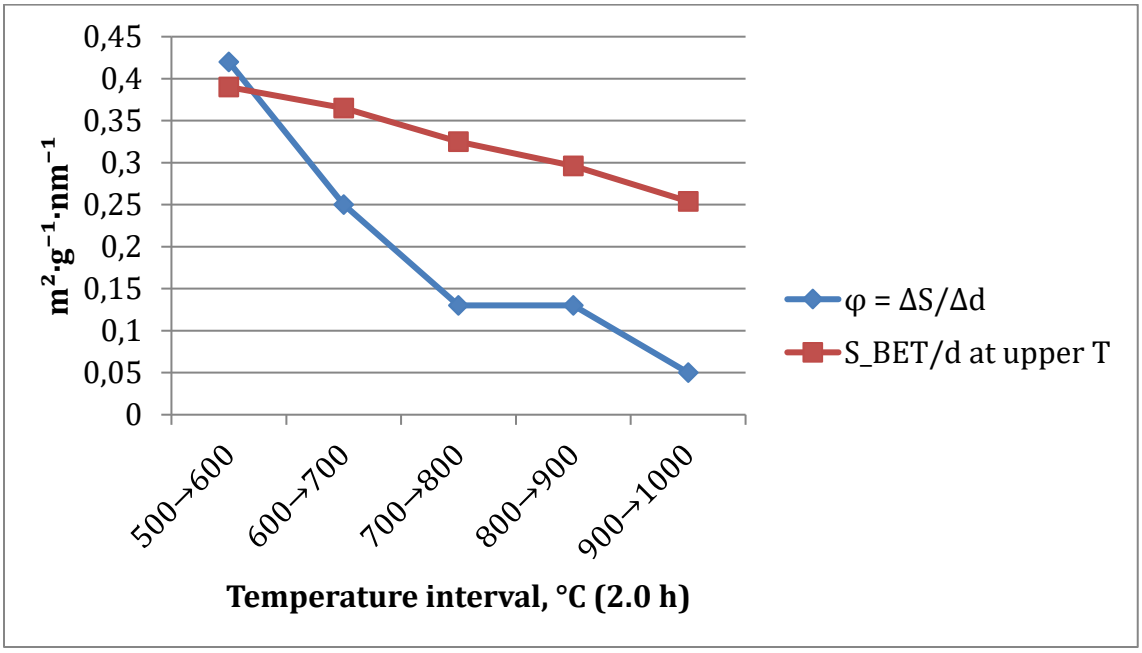


Fig. 5. Surface gained per nanometre of crystallite growth (φ) and cumulative ratio S_{BET}/d along the 2.0 h series.

The temperature at which φ collapses coincides with the range in which, according to published kinetics, the reconstructive transformation of maghemite to hematite becomes dominant . Oxidation of magnetite in air begins at low temperature with a topotactic step to γ-Fe_2O_3, which keeps the spinel lattice and its ferrimagnetism; the conversion to rhombohedral α-Fe_2O_3 requires lattice reconstruction, accelerates strongly between 600 and 900 °C and is complete near 1000 °C. Lattice reconstruction mobilises grain boundaries, which is the most plausible reason for the acceleration of crystallite growth (Δd per 100 °C rising from 9 to 19 nm) above 700 °C. The consequences for the sorbent are threefold: loss of lattice Fe^{2+} and hence of the reductive immobilisation of U(VI), Se and V; loss of the magnetisation needed for magnetic recovery ; and lengthening of diffusion paths in coarser grains. Although the phase ratio was not measured here, the convergence of the textural evidence with the oxidation kinetics is strong enough to treat ≈700 °C as the boundary beyond which thermal activation turns into oxidative degradation. XRD and magnetic-susceptibility measurements of the 700 °C product are recommended as the next step.

Taken together, the models point to 700 °C and 2.0 h as the upper practical limit of thermal activation rather than merely one acceptable regime. At this point the sorbent has 23.67 $m^2\ g^{-1}$ of BET surface — 84 % of what the thermal route can give at all — with 18.80 $m^2\ g^{-1}$ external, 0.120 $cm^3\ g^{-1}$ of pore volume and crystallites of 64.86 nm. Beyond it, each step of 100 °C buys 1–2 $m^2\ g^{-1}$ at the price of 13–19 nm of coarsening and of progressive hematite formation; the full 1000 °C would deliver the remaining 16 % of surface with crystallites 1.7 times larger. In time, the saturation analysis shows that holds longer than ≈1.0–1.4 h add little at any temperature; the 2.0 h hold is retained as a margin for the slower heating of bulk charges in an industrial kiln, while 2.5 h would add only 0.37 $m^2\ g^{-1}$ at 700 °C.

It is worth placing these values in perspective. Mechanical activation of the same ore reaches ≈94 $m^2\ g^{-1}$, more than three times the thermal maximum. The thermal step should therefore be seen not as the main source of surface but as the operation that stabilises the surface chemistry of finely ground material while leaving its magnetite core intact — a role it fulfils at 700 °C and loses above it. In the two-stage treatment scheme developed for Kyzylkum waters (lime pre-treatment to pH 7.5–8.0, then 4–6 g L^{-1} of sorbent), the activated material removed the target oxyanions in the order As > V > Mo > U > Se; the sorption results are reported separately.

Conclusion

Over a 6 × 5 grid (500–1000 °C, 0.5–2.5 h) the BET area of thermally activated Tebinbulak titanomagnetite is described by $S_{BET} = -83.1 + 15.8 \ln T + 3.60 \ln t$ ($R^2 = 0.976$). The time response is

first-order with $\tau = 0.31–0.45$ h, so that holds beyond ≈1.0–1.4 h add little; the limiting area rises from 17.2 to 27.8 $m^2 g^{-1}$ with diminishing increments per 100 °C.

Crystallite size follows $d \propto T^{1.31} t^{0.12}$ ($R^2 = 0.992$): coarsening is governed by temperature and is almost insensitive to time. External surface forms 75–80 % of the BET area and pore volume mirrors the area trend.

The surface gained per nanometre of crystallite growth falls eightfold between the 500→600 and 900→1000 °C steps, with the sharpest drop above 700 °C — the range in which the maghemite-to-hematite transformation of magnetite becomes dominant.

700 °C/2.0 h is the upper practical limit of thermal activation compatible with retention of the magnetite phase: 23.67 $m^2 g^{-1}$ (84 % of the thermal maximum), 18.80 $m^2 g^{-1}$ external, 0.120 $cm^3 g^{-1}$ pore volume, 64.86 nm crystallites.

Since the thermal route yields less than one third of the surface obtainable mechanically, it is recommended as a surface-stabilising step after fine grinding in the production of a magnetically separable oxyanion sorbent from this ore. Direct phase quantification by XRD and magnetic measurements of the 700 °C product are the next steps.

References

[1] M. Qadir, B. R. Sharma, A. Bruggeman, R. Choukr-Allah, and F. Karajeh, "Non-conventional water resources and opportunities for water augmentation to achieve food security in water scarce countries," Agricultural Water Management, vol. 87, pp. 2–22, 2007, doi: 10.1016/j.agwat.2006.03.018.

[2] P. Micklin, "The Aral Sea disaster," Annual Review of Earth and Planetary Sciences, vol. 35, pp. 47–72, 2007, doi: 10.1146/annurev.earth.35.031306.140120.

[3] R. Kulmatov, J. Mirzaev, J. Abuduwaili, and B. Karimov, "Challenges for the sustainable use of water and land resources under a changing climate and increasing salinization in the Jizzakh irrigation zone of Uzbekistan," Journal of Arid Land, vol. 12, pp. 90–103, 2020, doi: 10.1007/s40333-020-0092-8.

[4] R. S. Ayers and D. W. Westcot, Water Quality for Agriculture, FAO Irrigation and Drainage Paper 29, Rev. 1. Rome, Italy: FAO, 1985.

[5] R. Tornqvist, J. Jarsjo, and B. Karimov, "Health risks from large-scale water pollution: Trends in Central Asia," Environment International, vol. 37, pp. 435–442, 2011, doi: 10.1016/j.envint.2010.11.006.

[6] K. K. Tanji and N. C. Kielen, Agricultural Drainage Water Management in Arid and Semi-Arid Areas, FAO Irrigation and Drainage Paper 61. Rome, Italy: FAO, 2002.

[7] C. A. Hejase, K. A. Weitzel, S. C. Stokes, et al., "Opportunities for treatment and reuse of agricultural drainage in the United States," ACS ES&T Engineering, vol. 2, pp. 292–305, 2022, doi: 10.1021/acsestengg.1c00277.

[8] B. A. Manning, S. E. Fendorf, and S. Goldberg, "Surface structures and stability of arsenic(III) on goethite: Spectroscopic evidence for inner-sphere complexes," Environmental Science & Technology, vol. 32, pp. 2383–2388, 1998, doi: 10.1021/es9802201.

[9] S. Goldberg and C. T. Johnston, "Mechanisms of arsenic adsorption on amorphous oxides evaluated using macroscopic measurements, vibrational spectroscopy, and surface complexation modeling," Journal of Colloid and Interface Science, vol. 234, pp. 204–216, 2001, doi: 10.1006/jcis.2000.7295.

[10] D. Peak and D. L. Sparks, "Mechanisms of selenate adsorption on iron oxides and hydroxides," Environmental Science & Technology, vol. 36, pp. 1460–1466, 2002, doi: 10.1021/es0156643.

[11] J. P. Gustafsson, "Modelling molybdate and tungstate adsorption to ferrihydrite," Chemical Geology, vol. 200, pp. 105–115, 2003, doi: 10.1016/S0009-2541(03)00161-X.

[12] T. B. Scott, G. C. Allen, P. J. Heard, and M. G. Randell, "Reduction of U(VI) to U(IV) on the surface of magnetite," Geochimica et Cosmochimica Acta, vol. 69, pp. 5639–5646, 2005, doi: 10.1016/j.gca.2005.07.003.

[13] D. E. Latta, C. A. Gorski, M. I. Boyanov, E. J. O'Loughlin, K. M. Kemner, and M. M. Scherer, "Influence of magnetite stoichiometry on U(VI) reduction," Environmental Science & Technology, vol. 46, pp. 778–786, 2012, doi: 10.1021/es2024912.

[14] A. C. Scheinost and L. Charlet, "Selenite reduction by mackinawite, magnetite and siderite: XAS characterization of nanosized redox products," Environmental Science & Technology, vol. 42, pp. 1984–1989, 2008, doi: 10.1021/es071573f.

[15] C. A. Gorski and M. M. Scherer, "Influence of magnetite stoichiometry on Fe(II) uptake and nitrobenzene reduction," Environmental Science & Technology, vol. 43, pp. 3675–3680, 2009, doi: 10.1021/es803613a.

[16] C. T. Yavuz, J. T. Mayo, W. W. Yu, et al., "Low-field magnetic separation of monodisperse Fe_3O_4 nanocrystals," Science, vol. 314, pp. 964–967, 2006, doi: 10.1126/science.1131475.

[17] R. D. Ambashta and M. Sillanpää, "Water purification using magnetic assistance: A review," Journal of Hazardous Materials, vol. 180, pp. 38–49, 2010, doi: 10.1016/j.jhazmat.2010.04.105.

[18] J. T. Mayo, C. Yavuz, S. Yean, et al., "The effect of nanocrystalline magnetite size on arsenic removal," Science and Technology of Advanced Materials, vol. 8, pp. 71–75, 2007, doi: 10.1016/j.stam.2006.10.005.

[19] S. Goldberg, H. S. Forster, and C. L. Godfrey, "Molybdenum adsorption on oxides, clay minerals, and soils," Soil Science Society of America Journal, vol. 60, pp. 425–432, 1996, doi: 10.2136/sssaj1996.03615995006000020013x.

[20] J.-H. Huang, F. Huang, L. Evans, and S. Glasauer, "Vanadium: Global (bio)geochemistry," Chemical Geology, vol. 417, pp. 68–89, 2015, doi: 10.1016/j.chemgeo.2015.09.019.